# High-Entropy Alloy (HEA)-Coated Nanolattice Structures and Their Mechanical Properties

Libo Gao[1], Jian Song[1], Zengbao Jiao[2], Weibing Liao[1,4], Junhua Luan[1,5], James Utama Surjadi[1], Junyang Li[1], Hongti Zhang[1,5], Dong Sun, Chain Tsuan Liu[1,5], Yang Lu[1,5,6,*]

[1]Department of Mechanical and Biomedical Engineering, City Universityof Hong Kong, Hong Kong, China

[2]Department of Mechanical Engineering, Hong Kong PolytechnicUniversity, Hong Kong, China

[3]College of Physics and Energy, Shenzhen University, Shenzhen 518060, China

[4]Center for Advanced Structural Materials, City University of HongKong, Hong Kong, China

[5]Shenzhen Research Institute, City University of Hong Kong, Shenzhen518057, China

E-mail: yanglu@cityu.edu.hk

## Abstract

Nanolattice structure fabricated by two-photon lithography (TPL) is a coupling of size-dependent mechanical properties at micro/nano-scale with structural geometry responses in wide applications of scalable micro/nano-manufacturing. In this work, three-dimensional (3D) polymeric nanolattices are initially fabricated using TPL, then conformably coated with an 80 nm thick high-entropy alloy (HEA) thin film (CoCrFeNiAl0.3) via physical vapor deposition (PVD). 3D atomic-probe tomography (APT) reveals the homogeneous element distribution in the synthesized HEA film deposited on the substrate. Mechanical properties of the obtained composite

architectures are investigated via in situ scanning electron microscope (SEM) compression test, as well as finite element method (FEM) at the relevant length scales. The presented HEA-coated nanolattice encouragingly not only exhibits superior compressive specific strength of ≈0.032 MPa kg−1 m3 with density well below 1000 kg m−3, but also shows good compression ductility due to its composite nature. This concept of combining HEA with polymer lattice structures demonstrates the potential of fabricating novel architected metamaterials with tunable mechanical properties.

## 1. Introduction

Ordered micro/nanolattice is of intensive interest recently because of its tremendous potential in a wide range of applications, such as hierarchical structural materials, functional materials for sustainable energy, nano-scaffolds for cells culturing, etc. based on its unique and superior mechanical property compared to stochastic foams. This includes high strength and fracture toughness, low density, as well as high surface area to volume ratio deduced from the synergistic coupling effect between the geometrical structure and functional constituent materials.**1**-**9** The strength of lattices is determined not only by the order and periodicity of its structure, but also by the constituent materials.**10**, **11**Recently, numerous engineering materials such as Al2O3,**12**-**14** Ni–P alloy,**4**, **15**glassy carbon,**16** copper,**17** gold,**18** and metallic glass**19**, **20** have been employed as constituent materials to significantly enhance the mechanical properties of pristine polymer scaffolds with respect to its strength and

stiffness. Nevertheless, exploring a kind of lightweight, low-cost, and easily fabricated material with promising mechanical features that are easily to be coupled with pristine lattice structure is still a challenge.

As a new kind of alloys, high entropy alloys (HEAs) have recently aroused increasing attention due to their unique alloy design concept, tunable compositions, microstructures, and particularly, adjustable mechanical properties as compared to conventional metal/alloys in a wide range of engineering applications as functional and structural materials.**21**-**25** HEAs characteristic feature of entropy maximization to achieve phase stabilization allows them to obtain unique microstructures and exhibit promising properties.**26**-**28**CoCrFeNiAl0.3 HEA fiber fabricated by Li et al. exhibited an outstanding combination of strength and ductility, providing an innovative way to fabricate high performance engineering materials.**29** The tensile strength of single phase face-centered cubic (FCC) CrMnFeCoNi HEAs with exceptional damage tolerance was above 1 GPa, and fracture toughness values exceeded 200 MPa m1/2.**28** Noted that through reasonably adjusting the dominant structural form, HEA would exhibit alterable mechanical properties, this means. For example, HEA with mixture of body-centered-cubic (BCC) and FCC lattices, is expected to exhibit both balanced high strength and good ductility. This indicates that we can possibly fabricate the structure in catering to given application through tuning the constituent structure. Specially, certain interesting functional properties would be achieved for the HEA, while which cannot obtained by traditional alloy because of the cocktail effect.**21** These days, nanoscale size effects has been extensively studied

owing to the general trend in which materials obtain a substantial increase in strength by reducing their dimensions compared to their bulk ones.**30**, **31** For example, Zou et al. proved that the HEA at nanoscale exhibit extraordinarily high tensile strength and ductility compared to its bulk form.**23**Unfortunately, to date, no prior research pertaining to 3D nano/micro lattice in combination with nanoscale HEA has been reported yet. However, with the rapid advancement of sputtering techniques, HEA film fabricated at nanoscale can now be employed as the optimal coating material.**23**, **32**, **33** Likewise, Lee et al. has used the sputtering technique to successfully manufacture metallic glass nanolattices.**19** Additionally, the flexibility of two-photon lithography (TPL) allows countless number of different lattices with several orders of hierarchy and sizes to be fabricated.**12**, **34** By altering the design and material composition of these micro/nano-lattices, it is possible to produce a wide variety of materials with unprecedented properties that defies traditional mechanics, such as a strong, yet lightweight materials.**35**, **36** Rationally combining sputtering technique in preparation of HEA with TPL will possibly open an entirely new field of materials, which has the potential to reach theoretical limits and applications across multiple disciplines that would otherwise be impossible with macroscopic constructions.

Herein, we report, for the first time, the fabrication, characterization, and mechanical properties of HEA(CoCrFeNiAl0.3)-coated polymer composite nanolattices with the corresponding dimensions of individual structural components spanning across more than four orders of magnitude, from nanometers to tens of micrometers via TPL

combined with physical vapor deposition (PVD) route.**18**, **19** BCC topological structure is introduced, since its extensively experimentally and theoretically examined.**37** More importantly, the CoCrFeNiAl0.3 HEA thin film coating fabricated via radio frequency (RF) sputtering methodology has been developed and applied in nanolattice structures for the first time. Combining the merits of HEA and polymer nanolattice structures, the presented hybrid nanolattices exhibit superior compressive specific strength of 0.032 MPa kg−1 m3 with density below 1000 kg m−3, while still own an admirable compressive ability as compared to those made by pure metal/alloys.

## 2. Results and Discussion

Figure **1** schematically illustrates the fabrication process of the 3D composite nanolattice structures. Initially, a 3D structure was designed using the software Solidworks, a computer aided design (CAD) program, as shown in Figure **1**a. The designed structure file was then imported into the Nanowrite software for TPL direct laser writing. This method allows features down to the nanometer-scale to be produced. Once the polymer nanolattice was obtained (Figure **1**c), it was subsequently coated with a thin layer (≈80 nm) of HEA (CrFeCoNiAl0.3) film using sputter deposition, as shown in Figure **1**d. RF magnetron sputtering system was used here to deposit the film in a vacuum chamber at room temperature to finally obtain the composite nanolattices.

### 2.1 HEA Film

To gain a deep understanding on the composition and microstructure of the HEA film, the characterization of CrFeCoNiAl0.3 HEA film which was deposited on a Si wafer as the substrate under the same PVD condition that was performed in lattice coating (Figure **1**, the process of sputtering). Figure **2**a shows the field emission scanning electron microscope (FESEM) images of the HEA film on Si substrate as seen from the top. An extremely smooth surface with no aggregation of nanoparticles can be clearly seen. In situ nanoindentation was employed to test its mechanical properties with Young's modulus of 201.4 GPa and hardness of 11.46 GPa, which is much higher than its bulk counterpart,**38** as shown in Figure **2**a. Figure **2**b is the cross section FESEM image of the HEA film on the Si substrate, which shows that the thickness of the thin HEA film is ≈85 nm after depositing for 10 min. A smooth surface without columnar dendritic crystals can be observed. Figure S1 shows the XRD patterns of the fabricated HEA film, which identified the FCC crystal structure. All of these values match with the previously reported results.**38** In order to avoid the insensitiveness of XRD to secondary phases presented in small amount, high-energy synchrotron radiation X-ray scattering was employed as shown in Figure **2**c. The peak positions can also be indexed with respect to the FCC pattern. The subtle minor scattering peak indicates a low content of the secondary phase. This secondary phase has been identified to be NiAl-type ordered BCC phase by previous study, which is beneficial to the mechanical enhancement of the HEA film due to fact that the NiAl-type BCC phase is much harder than the matrix and presents a barrier to gliding dislocations.**29** Figure **2**d is the high-resolution transmission electron microscopy (HRTEM) image of the HEA film, which

shows the crystallization feature of the HEA film. More importantly, small nanocrystal can be distinctly observed. Inset in Figure **2**d is the corresponding select area electron diffraction (SAED) image, further confirming the crystallization feature. Normally, nano-grained metals show high strength and hardness due to the formation of nanocrystalline grains, which is favorable to the mechanical enhancement of the HEA film.[39, 40] 3D atomic-probe tomography (APT) and STEM-EDX (Figure S3) were employed to further characterize the element distribution and phase structure of the HEA film, as shown in Figure **2**e and f. Apparently, the Co, Cr, Fe, Ni, and Al found within the analyzed volume has a homogeneous distribution at nanoscale with no signs of segregation and clustering. In addition, the concentrations of various elements in the blue area (Figure **2**f) are in good agreement with our nominal composition in bulk specimen.

### 2.2 Polymer/HEA-Coated Composite Nanolattices

Figure **3** shows the morphology and dimensions of the fabricated hierarchical nanolattices. Figure **3**a exhibits the pristine polymer nanolattice, which was designed using a series of regular BCC unit structures connected at their vertices. Each individual BCC structure was made up of 8 struts, with the individual struts being ≈720 nm in diameter. The resulting structure was ≈20 μm in X and Y direction. From Figure **3**b, it can be observed that the polymer nanolattice was conformally coated with a thin HEA film without any obvious cracks during the process of sputtering. This is confirmed by the post-mortem FESEM images of the nanolattice composite, as shown in Figure **3**e,

and its corresponding digital optical images, which can be seen in Figure S2. The thickness of the HEA film is ≈83 nm, which is in accordance with Figure **2**b. Additionally, the characteristic nano-structural length scale of CoCrFeNiAl0.3, represented by its grain size, is between 5 and 20 nm, as can be seen in the TEM image in Figure **3**f. Figure **3** also contains a scale bar at the bottom, which indicates all relevant sizes within these structures, showing the hierarchical structure.

SEM-EDS was employed to further investigate the composition and distribution of the HEA film coating on the polymer nanolattice. Figure **4** shows the element distribution of the area which has been marked in Figure **4**a in red rectangle. Homogenous element distribution can be clearly seen throughout the whole topological structure. Furthermore, the atomic ratio of the Cr, Fe, Co, Ni, and Al shown in Figure **4**j is very close to 1:1:1:1:0.3, which is in accordance with the sputtering target in our experiment. Also, it was deduced that the Si element is mainly ascribed to the Si substrate while carbon and oxygen element are derived from the polymer core structure. The presented result further demonstrates the successful fabrication of the composite nanolattices structure.

Based on above discussion, the HEA-polymer nanolattice composite has been successfully fabricated. In situ uniaxial compression experiments in combination with FEM were then performed on the composite structure by applying an axial load along the vertical axes of the unit cells by using a flat punch indenter tip (Figure **5**a). Figure **5**b exhibits the SEM snapshot of the compression process of the composite nanolattice

structure, no evidence of obvious deformation was observed. Figure **5**h shows the averaged engineering stress–strain curves of the polymer and composite nanolattice. In these curves, the loading modulus ($E$) was defined as the slope in the linear elastic regime and the peak strength ($\sigma p$) was regarded as the maximum stress achieved by the structure before it collapsed. A nonlinear strain produced by the misalignment between the flat punch and top plane of the architecture structure was always observed, which had a minor effect on the overall mechanical response.**41** For the polymer nanolattice, an uniform plateau was observed in the stress after the elastic regime at ≈15% strain and 4 MPa. For the composite nanolattices, a linear region up to 11% at 7.76 MPa was observed, followed by a brittle failure at 12% (as shown in Figure **5**c–g). It is important to note that the stress–strain curve exhibit several structural instabilities, which is caused by the fracture of individual struts driven by the brittle HEA layers near or at the junctions (Figure **5**e–g). Failure in such structural materials is always initiated at the weakest connection, which is determined by the competing effects of stress concentrators at surface imperfections and local stresses within the microstructure landscape.**13** It is noted that a plateau stress can be clearly observed in polymer nanolattice, whereas a brittle-like behavior exists in composite nanolattices in which the failure of the structure with HEA film results in a drop in the stress-strain curve. This is due to the dominating buckling and brittle fracture mechanism for the bare polymeric nanolattice and composite nanolattices, respectively, as shown in Movie S1 and S2 in the supporting information.**12** Specifically, the enhancement principle can be associated with the HEA coating (shell) carries compressive forces while the polymer

core used to resist early surface cracking and to increase toughness. However, when the core is not still enough to increase the compressive capability and the buckling stress is dominated by the buckling stress of the shell.**42** Meanwhile, the HEA is in the ductile-to brittle transition due to the size effects.**41** Therefore, a brittle behavior would be observed at a certain point, which is in good agreement with other reports.**12**, **41**, **42** To demonstrate the important role of the polymer core in the composite nanolattices, a loading-unloading compression test was employed (Figure S4). As shown in the exhibited mechanical behaviors, nearly the same Young's modulus ($74.5 \pm 3.5$ MPa) was observed, indicating the superior recoverability of the composite nanolattices under an applied strain of nearly 8%. In addition, the nanolattice show similar viscoelasticity behavior, due to the existed polymeric core.**43** It is worth mentioning that the composite nanolattices exhibit superior compressive strain, which possibly due to the polymeric core supporting. Finally, through these data, it can be calculated that the specific compressive strength of the presented composite nanolattices is 0.032 MPa kg−1 m3, which is comparable even higher than that of the micro/nano lattice reported before, for instance, polymer/NiB (0.017 MPa kg−1 m3),**41** polymer/Si3N4 (0.012 MPa kg−1 m3),**42** and SiC microlattices (≈0.023 MPa kg−1 m3)**44** and a detailed comparison can be found in Table S1, demonstrating the superior mechanical properties of the composite nanolattices based on the synergistic effect between polymer and HEA film.

Thin films, both amorphous and crystalline films, have been extensively reported to be capable of enhancing the performance of many types of materials through coating,

especially the mechanical performance of substrate materials.**41**, **45**-**47**Furthermore, scaling down a material structure down to the nanoscale can cause them to exhibit different behaviors, as compared to their bulk counterparts, in which they become stronger as their size is reduced according to the Hall–Petch relationship.**23**, **48**, **49** Therefore, it is hypothesized that a thin HEA film at nanoscale may greatly enhance the mechanical performance of the composite micro/nano structure. It is, therefore, recognized that the unique superior performance of our composite nanolattice can be ascribed to the thin HEA film with promising mechanical performance at nanoscale and the "size effect" of the structural geometry size. Additionally, for the polymer core, which is sufficiently stiff to support the outer shell bearing the weight, enhanced the strain of the nanolattice composite structure, causing it to outperform some composite nanolattices reported before. Importantly, to further investigate the compressive behavior of fabricated nanolattices, Finite Element Method (FEM) was also conducted to benchmark with the experimental results, as shown in Figure S5 and S6. The corresponding results obtained by FEM reveal that the maximum stress location and stress distribution in each step, and the prediction values, that is, modulus and strength, and stress–strain curves are in good agreement with the corresponding tests. Such simulation approach can be used to further refine the hybrid nanolattice structure design and tune its anisotropic mechanical properties for specific applications.

## 3. onclusion

In summary, we have successfully demonstrated the first 3D hybrid HEA-coated nanolattice structures with the characteristics feature sizes spanning from 5 nm to 20 μm. To achieve this novel structural metamaterial, the RF sputtering methodology was employed to deposit HEA (CoCrFeNiAl0.3) thin film for the first time. In situ SEM compression test demonstrated that the fabricated composite nanolattices possess high compressive strength of 0.032 MPa kg−1 m−3 with density well below 1000 kg m−3 and reasonably good compression ability due to its composite nature. The design concept of combining HEA with polymer lattice structure, coupled with the programmable versatility of TPL, will possibly lead to new insights in developing tunable mechanical metamaterials with potential applications in structural engineering, flexible electronics as well as biomedical instruments.

## 4. Methods

### 4.1 Fabrication of the HEA-Coated Hybrid Nanolattices

Firstly, standard CAD software was employed to design the individual lattice units with specified BCC geometries. FEM analysis of the designed structure was conducted to estimate its mechanical properties and help to provide the optimum design and geometries. The polymer nanolattice scaffold was initially fabricated using TPL direct laser writing process in IPL-780 photoresist via using the Photonic Professional lithography system (Nanoscribe™ GmbH). The size of the BCC structure is 20 × 20 × 10 μm. The IPL-780 photoresist was exposed to a 780 nm femtosecond

pulsed laser to fabricate the polymer structure. For the nanolattice described here, the optimum laser power was found to be 30 mW. The fabricated structure was then developed for 30 min in propylene glycol mono-methyl ether acetate (PGMEA), followed by rinsing in isopropyl alcohol for 5 min. RF magnetron was then used to conformally deposit thin HEA film at nanoscale on the polymer nanolattices at $1 \times 10{-}6$ Pa. The ignition argon flow was set to be 22 standard cubic centimeters per minute (sccm), while the total flow of argon flow rate was fixed at 12 sccm for 10 min at 500 W. Note that during the deposition procedure, the substrate was rotated at a rate of 2 rpm min−1 to guarantee homogeneous film distribution.

### 4.2 Microstructure and Composition Characterization

The element and morphology analysis of the nanolattice was observed by FESEM (FEI™, Quanta FEG450) and JEOL JSM 5600 equipped with Oxford EDX, transmission electron microscope (JEOL JEM 2100) equipped with SAED, and X-ray powder diffractometer (RigakuSmartLab™) with monochromatic Cu *Ka* radiation (l¼1.5418 Å). TEM foils were prepared through ion-milling at a temperature of −50 °C to avoid crystallization. The APT characterizations were performed in a local electrode atom probe (CAMEACA™ LEAP 5000 R). Needle-shaped specimens required for APT were fabricated by lift-outs and annular milled in a FEI Scios™ focused ion beam/scanning electron microscope (FIB/SEM). The specimens were analyzed at 70 K in voltage mode, a pulse repetition rate of 125 kHz, a pulse fraction of 20%, and an evaporation detection rate of 0.2% atom per pulse. Imago Visualization and Analysis

Software (IVAS) version 3.6.12 was used for creating the 3D reconstructions and data analysis.

### 4.3 In Situ SEM Mechanical Characterization

Monotonic and cyclical uniaxial compression experiments were performed on the nanolattices inside SEM through a quantitative picoindentor (HysitronTM PI85). Nanolattices were compressed using a diamond flat punch tip with 120 μm in diameter, with the load applied from the apex of the vertical axis, moving down at a constant prescribed displacement rate of 10 nm s−1. Load-displacement curves were recorded. By using the nominal cross-sectional area and height of the whole structure, engineering stress and strain were obtained.


### Acknowledgements

The authors gratefully thank the funding supports from Shenzhen Science and Technology Innovation Committee under the grants JCYJ20160401100358589 and JCYJ20170413141157573. Part of this project was supported by the Research Grants Council of the Hong Kong Special Administrative Region of China (GRF No. CityU11216515) and City University of Hong Kong (Project Nos. 9667117 and 9667153). D.S. acknowledges the funding from RGC under the project GRF CityU11211714. The APT research was supported by the Collaborative Research Fund (CRF No. C1027-14E) from the Research Grant Council of Hong Kong.


### References

[1] N.A.Fleck,V.S.Deshpande,M.F.Ashby,Proc.R.Soc.AMath.Phys. Eng. Sci. 2010, 466, 2495.

[2] L.Valdevit,A.J.Jacobsen,J.R.Greer,W.B.Carter,J.Am.Ceram.Soc. 2011, 94, 15.

[3] V. S. Deshpande, N. A. Fleck, M. F. Ashby, J. Mech. Phys. Solids 2001, 49, 1747.

[4] T. A. Schaedler, A. J. Jacobsen, A. Torrents, A. E. Sorensen, J. Lian, J. R. Greer, L. Valdevit, W. B. Carter, Science 2011, 334, 962.

[5] A. Maggi, J. Allen, T. Desai, J. R. Greer, Extreme Mech. Lett. 2017, 13, 1.

[6] J.B.Berger,H.N.G.Wadley,R.M.Mcmeeking,Nature2017,543,533. [7] C. Peters, M. Hoop, S. Pan_x0019_e, B. J. Nelson, C. Hierold, Adv. Mater.

2016, 28, 533.

[8] V. F. Chernow, H. Alaeian, J. A. Dionne, J. R. Greer, Appl. Phys. Lett.

2015, 107, 101905.

[9] Z. Qin, G. S. Jung, M. J. Kang, M. J. Buehler, Sci. Adv. 2017, 3, 1.

[10] K. J. Maloney, C. S. Roper, A. J. Jacobsen, W. B. Carter, L. Valdevit, T. A. Schaedler, APL Mater. 2013, 1, 22106.

[11] Y. F. Zhou, C. Z. Yao, Q. L. Yang, L. Guo, L. Jiang, Adv. Eng. Mater. 2016, 18, 236.

[12] J. Bauer, S. Hengsbach, I. Tesari, R. Schwaiger, O. Kraft, Proc. Natl. Acad. Sci. 2014, 111, 2453.

[13] D. Jang, L. R. Meza, F. Greer, J. R. Greer, Nat. Mater. 2013, 12, 893. [14] L. R. Meza, S. Das, J. R. Greer, Science (80-.) 2014, 345, 1322.

[15] X. Zheng, H. Lee, T. H. Weisgraber, M. Shusteff, J. DeOtte,

E. B. Duoss, J. D. Kuntz, M. M. Biener, Q. Ge, J. A. Jackson, S. O. Kucheyev, N. X. Fang, C. M. Spadaccini, Science 2014, 344, 1373.

[16] J.Bauer,A.Schroer,R.Schwaiger,O.Kraft,Nat.Mater.2016,15,438. [17] X. Wendy Gu, J. R. Greer, Extreme Mech. Lett. 2015, 2, 7.

[18] L. C. Montemayor, L. R. Meza, J. R. Greer, Adv. Eng. Mater. 2014,

16, 184.

[19] S.W.Lee,M.Jafary-Zadeh,D.Z.Chen,Y.W.Zhang,J.R.Greer,Nano

Lett. 2015, 15, 5673.

[20] J. Rys, L. Valdevit, T. A. Schaedler, A. J. Jacobsen, W. B. Carter,

J. R. Greer, Adv. Eng. Mater. 2014, 16, 889.

[21] Y. Zhang, T. T. Zuo, Z. Tang, M. C. Gao, K. A. Dahmen, P. K. Liaw,

Z. P. Lu, Prog. Mater. Sci. 2014, 61, 1.

[22] Z. An, H. Jia, Y. Wu, P. D. Rack, A. D. Patchen, Y. Liu, Y. Ren, N. Li,

P. K. Liaw, Mater. Res. Lett. 2015, 3, 203.

[23] Y. Zou, H. Ma, R. Spolenak, Nat. Commun. 2015, 6, 7748.

[24] Y. Ma, G. J. Peng, D. H. Wen, T. H. Zhang, Mater. Sci. Eng. A 2015,

621, 111.

[25] H. Zhang, K. W. Siu, W. Liao, Q. Wang, Y. Yang, Y. Lu, Mater. Res.

Express 2016, 3, 1.

[26] Y. Zhang, X. Yang, P. K. Liaw, JOM 2012, 64, 830.

[27] Z. Li, K. G. Pradeep, Y. Deng, D. Raabe, C. C. Tasan, Nature 2016,

534, 227.

[28] B. Gludovatz, A. Hohenwarter, D. Catoor, E. H. Chang, E. P. George,

R. O. Ritchie, Science (80-.). 2014, 345, 1153.

[29] D. Li, C. Li, T. Feng, Y. Zhang, G. Sha, J. J. Lewandowski, P. K. Liaw,

Y. Zhang, Acta Mater. 2017, 123, 285.

[30] M.D.Uchic,D.M.Dimiduk,J.N.Florando,W.D.Nix,Science(80-.).

2004, 305, 986.

[31] J. Y. Kim, D. Jang, J. R. Greer, Acta Mater. 2010, 58, 2355.

[32] B. R. Braeckman, F. Boydens, H. Hidalgo, P. Dutheil, M. Jullien,

[41] M. Mieszala, M. Hasegawa, G. Guillonneau, J. Bauer, R. Raghavan, C. Frantz, O. Kraft, S. Mischler, J. Michler, L. Philippe, Small 2016, 13,

A.-L. Thomann, D. Depla, Thin Solid Films 2015, 580, 71. 1.

[33] B. R. Braeckman, D. Depla, J. Alloys Compd. 2015, 646, 810.

[34] R. L. Truby, J. A. Lewis, Nature 2016, 540, 371.

[35] X. Zheng, W. Smith, J. Jackson, B. Moran, H. Cui, D. Chen, J. Ye,

N. Fang, N. Rodriguez, T. Weisgraber, C. M. Spadaccini, Nat. Mater.

2016, 15, 1100.

[36] D. W. Yee, M. D. Schulz, R. H. Grubbs, J. R. Greer, Adv. Mater. 2017,

29, 1605293.

[37] S. Merkt, C. Hinke, J. Bültmann, M. Brandt, Y. M. Xie, J. Laser Appl.

2015, 27, S17006.

[38] S. G. Ma, S. F. Zhang, J. W. Qiao, Z. H. Wang, M. C. Gao, Z. M. Jiao,

H. J. Yang, Y. Zhang, Intermetallics 2014, 54, 104.

[39] T. H. Fang, W. L. Li, N. R. Tao, K. Lu, Science (80-.) 2011, 331, 1587.

[40] K. Lu, L. Lu, S. Suresh, Science (80-.) 2009, 324, 349.

[42] Y. F. Zhou, C. Z. Yao, Q. L. Yang, L. Guo, L. Jiang, Adv. Eng. Mater. 2016, 18, 236.

[43] A. Bravo, R. Rony, V. Tita, Mater. Res. 2006, 9, 327.

[44] S. Chabi, V. G. Rocha, E. Garcia-Tunton, C. Ferraro, E. Saiz, Y. Xia,

Y. Zhu, ACS Nano 2015, 10, 1871.

[45] J. P. Chu, J. E. Greene, J. S. C. Jang, J. C. Huang, Y. L. Shen, P. K. Liaw,

Y. Yokoyama, A. Inoue, T. G. Nieh, Acta Mater. 2012, 60, 3226. [46] H.Jia,F.Liu,Z.An,W.Li,G.Wang,J.P.Chu,J.S.C.Jang,Y.Gao,

P. K. Liaw, Thin Solid Films 2014, 561, 2.

[47] J.P.Chu,T.Y.Liu,C.L.Li,C.H.Wang,J.S.C.Jang,M.J.Chen,

S. H. Chang, W. C. Huang, Thin Solid Films 2014, 561, 102. [48] E. O. Hall, Proc. Phys. Soc. Sect. B 1951, 64, 747.

[49] N. J. Petch, J. Iron Steel Inst. 1953, 173, 25.

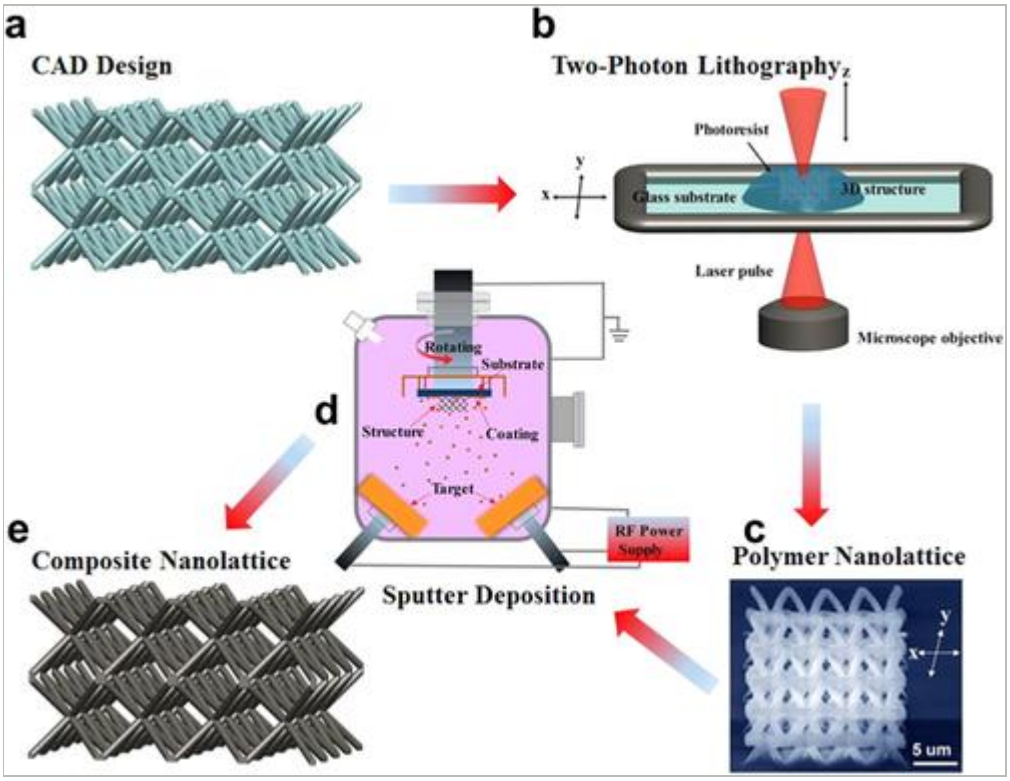


**Figure 1.**Schematic illustration of the fabrication of the HEA-coated nanolattice structures. a) CAD structures design used in this research. b) Fabrication procedure of pure polymer nanolattice via TPL. c) SEM images of 4 × 4 × 2 polymer nanolattice. d) Coating HEA thin film on polymer nanolattice through RF sputtering and e) the final composite nanolattice coated with HEA.

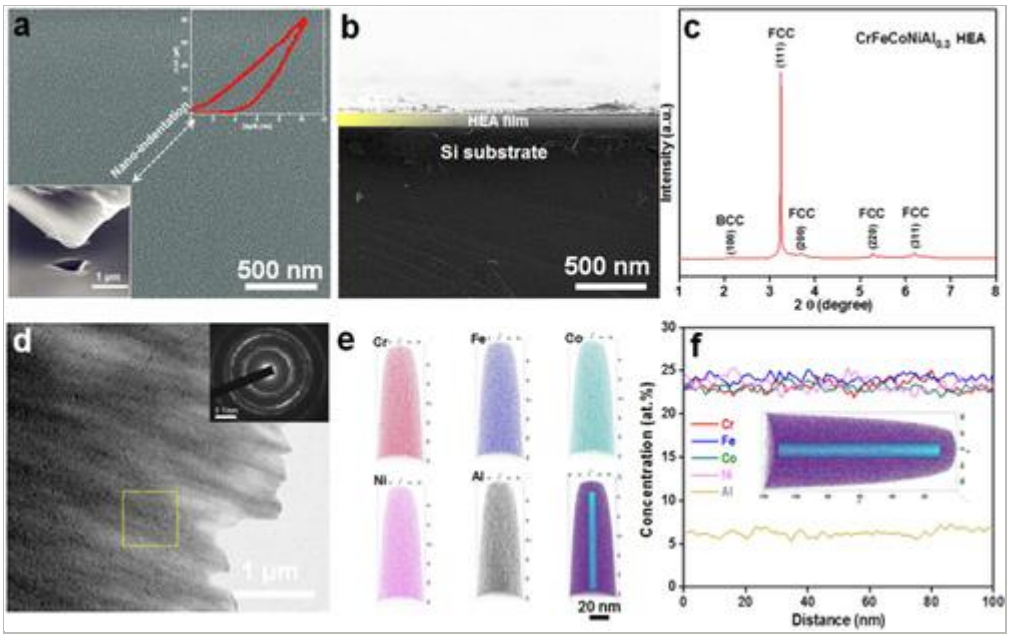


**Figure 2.**Microstructure and mechanical characterization of the as-deposited HEA film. a) SEM images of the surface of HEA deposited on Si substrate. Inset is the SEM images of nanoindentation and corresponding curves of load versus depth. b) SEM images of the cross section of 80 nm thick HEA deposited on Si substrate. c) Synchrotron radiation X-ray was used to characterize the phase structure of the as-deposited films. d) Representative TEM image and corresponding SAED pattern. e) 3D APT probing reconstructions of Cr, Fe, Co, Ni, Al atom positions. f) Concentrations of the elements plotted along the blue cylinder is in good agreement with nominal atomic ratio.

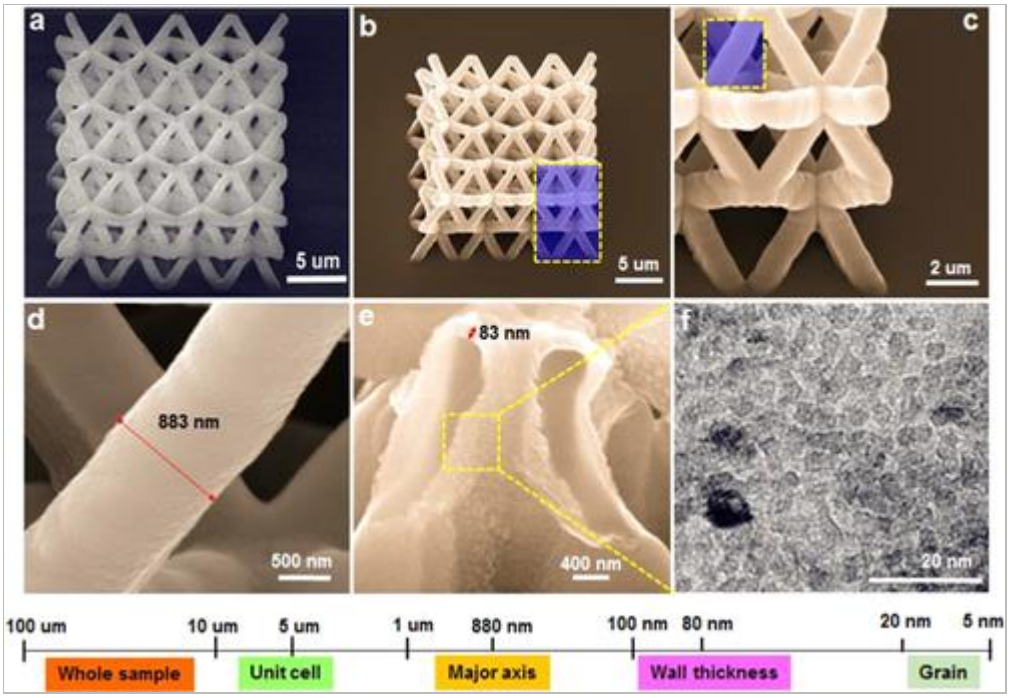


**Figure 3.**Hierarchical structure of the composite nanolattice, with the characteristic feature sizes spanning from 10 nm to 20 µm. a) Primary polymer nanolattice. b) Nanolattice coated with HEA thin film and c) d) a single strut with 883 nm in diameter. e) The thickness of the HEA is about 80 nm. f) TEM images of the HEA with 5–20 nm grain size.

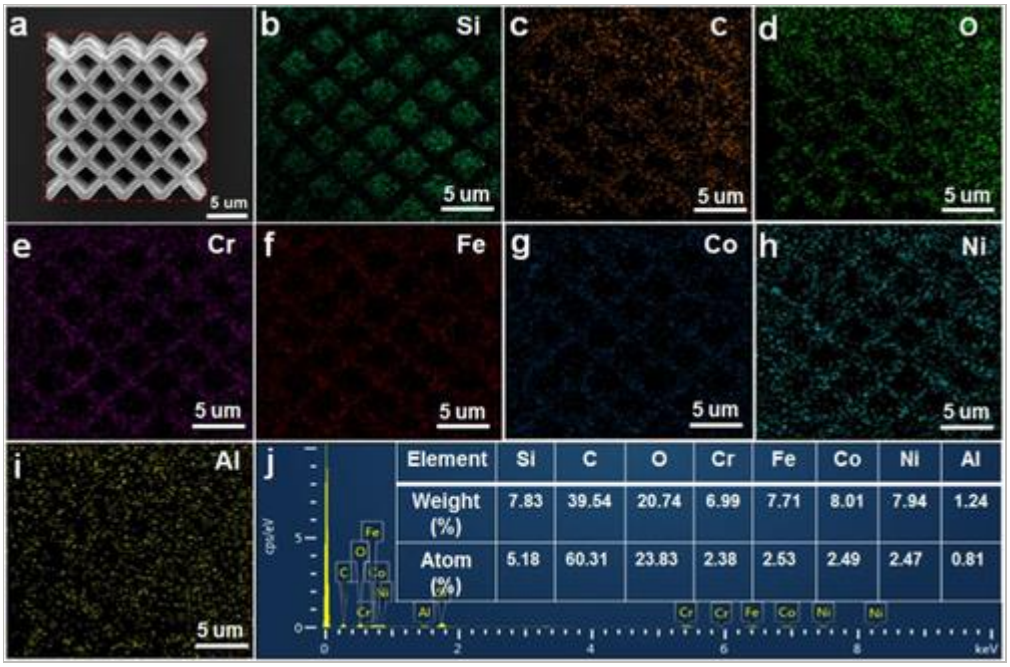


**Figure 4.**SEM-EDS mapping and element spectrum, indicating the homogeneous coating of HEA over the nanolattice structure.

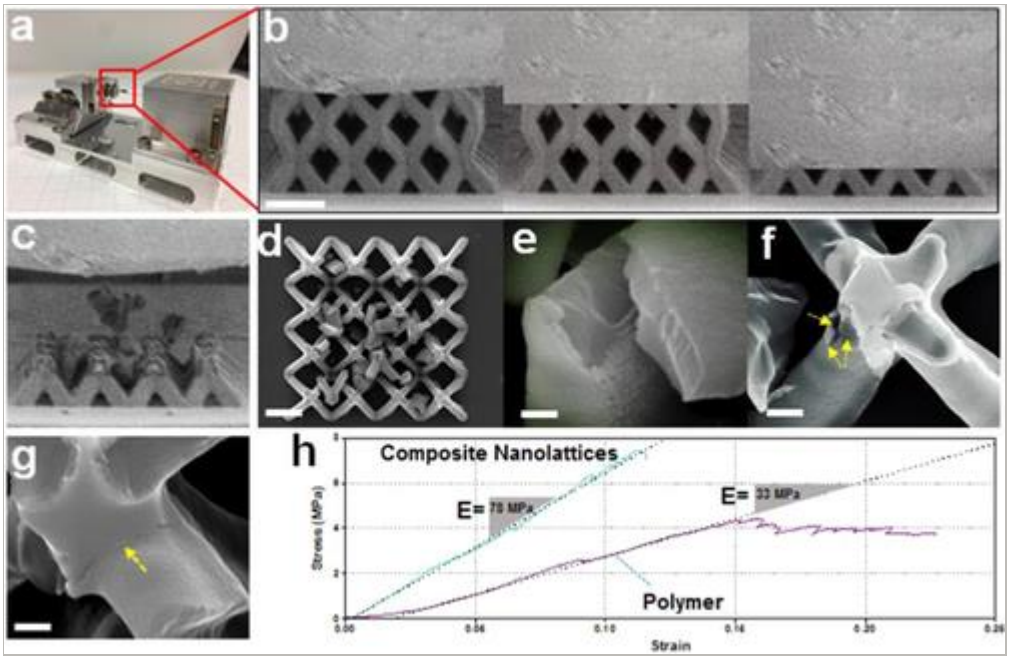


**Figure 5.**Compression tests on a HEA-coated nanolattice structure.(a) In situ SEM compression test set up for testing the composite nanolattice. b) Screenshot SEM images of the composite nanolattice during the compression test (side view). c, d) Side and top view of crushed composite nanolattice structure after compression test. e–g) Close-up view of a shell fragment from d). h) Stress–strain plots of a polymer-only nanolattice and a composite nanolattice that were tested under the same condition. The scale bars in b–d) is 5 μm and 500 nm in e–g), respectively.